Journal of Power Sources 196 (2011) 8180–8187

Contents lists available at ScienceDirect

Journal of Power Sources

journal homepage: www.elsevier.com/locate/jpowsour

CFD prediction of shunt currents present in alkaline fuel cells

Ge Zhou [a], Lea-Der Chen [b,*], James P. Seaba [c]

[a] UTC Power, 195 Governor's Highway, South Windsor, CT 06074, USA
[b] Texas A&M University – Corpus Christi, Corpus Christi, TX 78412, USA
[c] ConocoPhillips Co., 240 PLB, Bartlesville Technology Center, Bartlesville, OK 74004, USA

ARTICLE INFO

Article history:
Received 10 March 2011
Received in revised form 11 April 2011
Accepted 13 April 2011
Available online 22 April 2011

Keywords:
Alkaline fuel cell
Non-ideal solution
Shunt currents
Electric field potential

ABSTRACT

A CFD study was conducted for the electrolyte transport in a single-cell alkaline fuel cell. The transport model that accounts for the balance of mass, momentum, energy, species and electric charge in the electrolyte was solved. The CFD results captured the presence of primary and secondary (shunt) currents in the liquid electrolyte. The shunt currents were present in the regions adjacent to the separator inlet and exit, but not inside the separator nor in the extended channels. The calculated local shunt current density in the corner regions of the separator inlet and exit was higher than the average primary current. The results also showed that the IR loss due to the electric potential drop at high current densities is comparable to the overpotential loss at the anode. Passive and active mitigation measures against the shunt currents were suggested.

1. Introduction

A stationary fuel cell is a viable option for electrical power generation from renewable sources. For example, H_2 produced by solar or wind turbine based electrolysis can be used to fuel the fuel cells. Among the fuel cell platforms, the alkaline fuel cell (AFC) remains a good prospect as it has high reliability and it can use non-precious metal for the electrodes [1–7]. However, to be competitive with other power sources, the power density (as well as the cost of manufacturing, operation and maintenance) needs to be improved. In [8], it is shown that maintaining a uniform electrolyte concentration is an effective strategy to increase the limiting current density. Another technology challenge is corrosion due to the presence of shunt currents. Mathematical models describing the electrochemical and transport processes in AFC electrolytes are available; for example, see [9–15]. However, the transport models were formulated assuming ideal solutions. In [8] it is shown that the ideal solution formulation underestimates the limiting current density by 50% for the concentrated electrolyte condition considered, 7 M. Furthermore, the effects of temperature on transport properties were also neglected, which was shown to underestimate the limiting current density by 30% when compared to an adiabatic boundary condition [8]. In this paper, the ideal solution and isothermal assumptions were relaxed and a CFD calculation was performed for prediction of the presence of shunt currents in alkaline fuel cells.

Shunt currents or bypass currents are present in liquid electrolytes, coolant circuits of fuel cell stacks, and bipolar electrolyzers [6,16–23]. The presence of shunt currents is the result of an electric potential gradient along a common electrolyte path that forms a driving force for the net ionic fluxes. Shunt currents are not desired as they lead to corrosion problems, reduced service life, and system power losses. Shunt currents can be reduced or eliminated by applying (a) a protective current against the shunt current direction, (b) protective coatings on surfaces of the electrolyte/coolant channels, or (c) baffle plates to stop the ionic fluxes. Understanding the transport phenomena in electrolytes can help design considerations for effective mitigation measures. To model the current transport, models based on equivalent electrical circuits [24–28] or Laplace equations [29–32] are developed. To further the state of knowledge, a transport model that accounts for the balance of mass, momentum, energy, species, and charge in electrolytes and electrodes, and that satisfies the thermodynamic constraints of H_2 and O_2 dissolving in electrolytes is implemented in this study. The objective of this paper is to conduct a CFD based study of the electrochemical and transport processes in electrolytes, to gain insights into the presence of shunt currents in AFCs, and to provide suggestions that aid in design considerations.

2. Formulation

The assumptions invoked in the formulation are (a) Newtonian fluid, (b) negligible pressure effects on enthalpy, (c) negligible magnetic effects due to electric field, (d) negligible pressure and temperature effects on diffusion transport, (e) negligible viscous dissipation, pressure work, and Dufour effects in energy

* Corresponding author. Tel.: +1 361 825 3046; fax: +1 361 825 3056.
E-mail address: ldchen@tamucc.edu (L.-D. Chen).

0378-7753/$ – see front matter © 2011 Elsevier B.V. All rights reserved.
doi:10.1016/j.jpowsour.2011.04.029

Nomenclature

C	Molar concentration (kmol m^{-3})
F	Faraday constant (C kmol^{-1})
i	Current density (A m^{-2})
$\boldsymbol{i}$	Vector quantity of current density (A m^{-2})
R_u	Universal gas constant (J kmol^{-1} K^{-1})
$S^i_{\beta\sigma}$	Source term of Eq. (1)
T	Temperature (K)
t	Transference number
x	Coordinate, cross-stream direction (Fig. 1)
y	Coordinate, streamwise direction (Fig. 1)

Greek

δ	Dimensionless distance; $\delta = 0$ and 1 denotes separator inlet and exit, respectively
$\Delta\Phi$	Electric potential drop (V)
η	Overpotential (V)
$\gamma_{\pm,C}$	Mean activity coefficient based on molarity
κ	Electrical conductivity (S m^{-1})
κ^D	Diffusional ionic conductivity (A m^{-1})
Φ	Electrical potential at electrolyte phase (V)

Subscripts

a	Anode
c	Cathode
e	Electrolyte
β	Liquid phase
σ	Solid phase
0	Solvent
$-$	Anion

Superscripts

eff	Effective
D	Diffusion
i	Charge
0	Reference state

equation, (f) no homogeneous chemical reactions, (g) electroneutrality, (h) homogeneous and continuous media for gas and liquid phase, (i) local thermal equilibrium, (j) vapor–liquid equilibrium at the gas–liquid interface, and (k) negligible electrical resistance of the electrodes. The governing equations describing the transport of mass, momentum, species, energy and charge balance are given in [8], which account for (a) mass and species addition or removal due to gas solubility and H_2O phase change, (b) momentum exchange due to Darcian flow in porous electrodes, (c) energy source or sink terms due to heat and entropy generation at catalyst layers, Joule heating in separator and catalyst layers, and latent heat due to H_2O phase change, and (d) charge generation at catalyst layers. The constitutive equations describing the reaction rate (Butler–Volmer equation), capillary pressure (Leverett-J function), and physical properties are given in [8]. Species equation of the liquid phase is solved only for OH^-. The K^+ concentration is calculated from electroneutrality.

3. Solution method

The computational domain was divided into seven regions (domains) as illustrated in Fig. 1. Domains 1, 2, and 3 are the anode gas channel, gas diffusion layer (GDL), and catalyst layer, respectively. Domain 4 is the separator. Domains 5, 6, and 7 are the cathode catalyst layer, GDL, and gas channel, respectively. To solve the coupled nonlinear governing equations, FLUENT© software is utilized. The user defined functions (UDFs) were used for calculation of the physical properties and the source terms of the governing equations, and to satisfy the prescribed boundary conditions. The graphical user interface (GUI) was used to input the UDFs to the corresponding governing equations. The user defined scalar (UDS) was introduced to solve the charge equation. Two convergence criteria were enforced to ensure that (a) the local cell voltage is the same everywhere along the separator, and (b) the total current density equals that calculated by the specified, averaged cell current density. Description of the computational method and validation of the CFD results are given in [8].

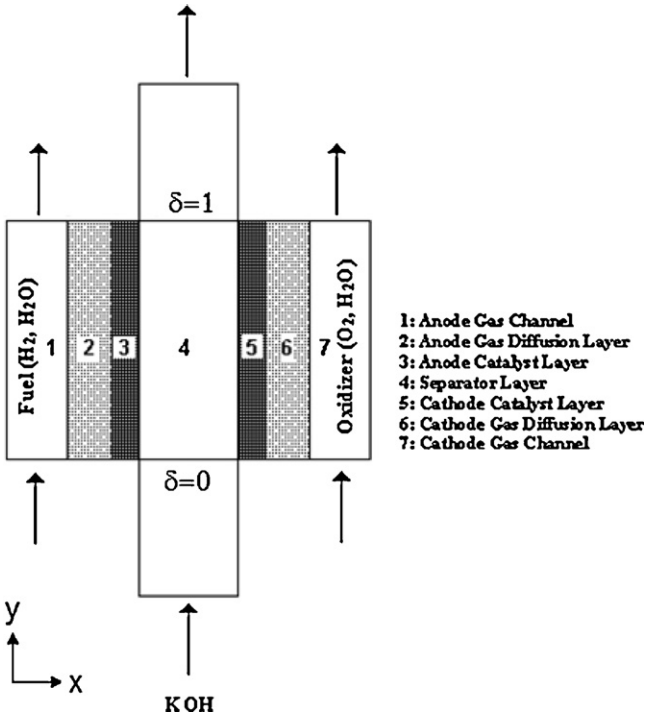

Fig. 1. Schematic of alkaline fuel cell.

4. Results and discussion

The primary and secondary (shunt) currents are calculated by charge balance equation [8]:

$$\nabla \cdot (\kappa_\beta^{\text{eff}} \nabla \Phi_\beta) + \nabla \cdot (\kappa_\beta^{D,\text{eff}} \nabla \ln C_{\beta e}) = S^i_{\beta\sigma} \tag{1}$$

The source term in the charge equation is used to calculate the charge transfer between the solid and liquid phase. The current density, i, is calculated from [8]:

$$i = -\kappa \nabla \Phi - \kappa^D \nabla \ln C_e \tag{2}$$

where κ is the electrical conductivity, Φ the electric potential, C_e the electrolyte molar concentration, and κ^D the diffusional ionic conductivity [33] or diffusion conductivity in short. The diffusion conductivity, which is associated with the ionic transport due to the presence of a concentration gradient, is calculated by:

$$\kappa^D = \left(\frac{2R_u T \kappa}{F}\right)\left(\frac{1 - t_-^0 + C_e}{2C_0}\right)\left(\frac{1 + d\ln\gamma_{\pm,C}}{d\ln C_e}\right) \tag{3}$$

where R_u is the universal gas constant, T the temperature, F the Faraday constant, t_-^0 the reference state transference number of negative ion, and $\gamma_{\pm,C}$ the mean molar activity coefficient. Constant and uniform electric potential is assumed for the electrodes; namely $\Phi_\sigma = 0$ and E_{cell} for the anode and cathode, respectively.

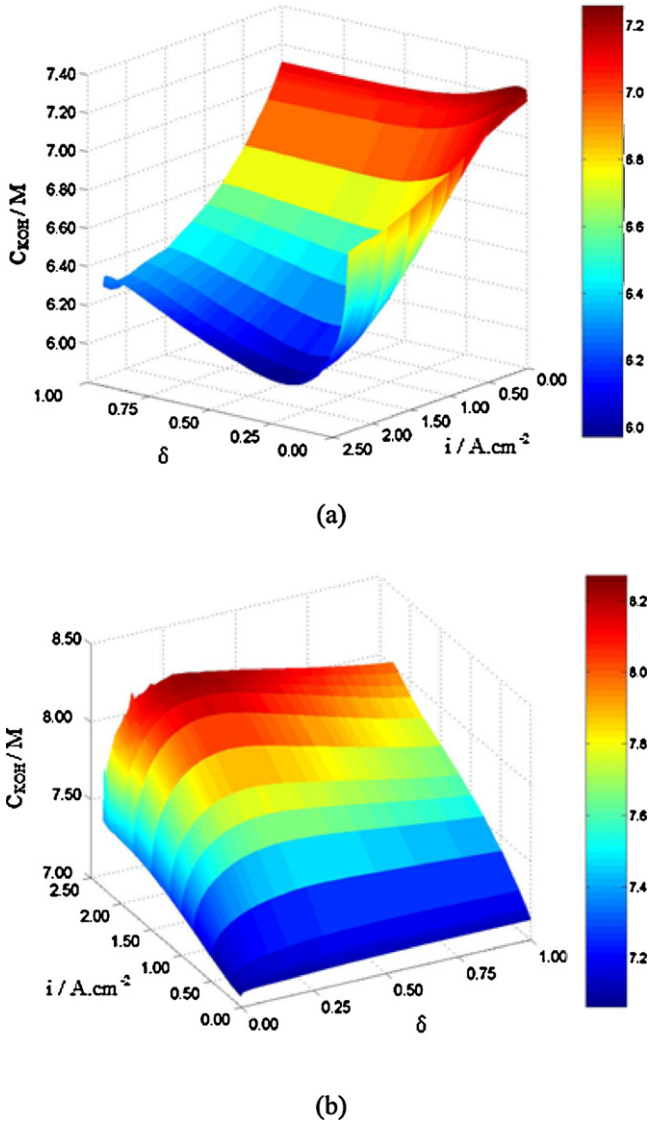

Fig. 2. KOH concentration along the electrodes (δ = 0 and 1 denotes separator inlet and exit, respectively) at specified average current density, adiabatic boundary condition; (a) anode and (b) cathode.

Electrolyte concentration and electric potential are solved in the CFD calculation. The primary and shunt currents are calculated accordingly.

For the computation, the baseline condition given in Table 6 of [8] was used unless noted otherwise. In short, the KOH concentration and temperature were set to 7 M and 80 °C at the separator inlet, respectively. The system pressure was set to 4.1 atm, and with pure H_2 and O_2 as the fuel and oxidant. The relative humidity of H_2 and O_2 was set to 0%. The anode, cathode and electrolyte velocities at the separator inlet were set to 0.2, 0.1, and 0.01 m s^{-1}, respectively. An adiabatic boundary condition was imposed.

4.1. Electrolyte concentration

The electrolyte concentration distributions along anode and cathode catalyst layers at specified current densities are shown in Fig. 2(a) and (b), respectively. At fixed streamwise locations (δ), the KOH concentration at anode decreases with increasing current density. This trend is expected as OH^- is consumed at anode. The KOH concentration was below the specified 7 M at the separator inlet

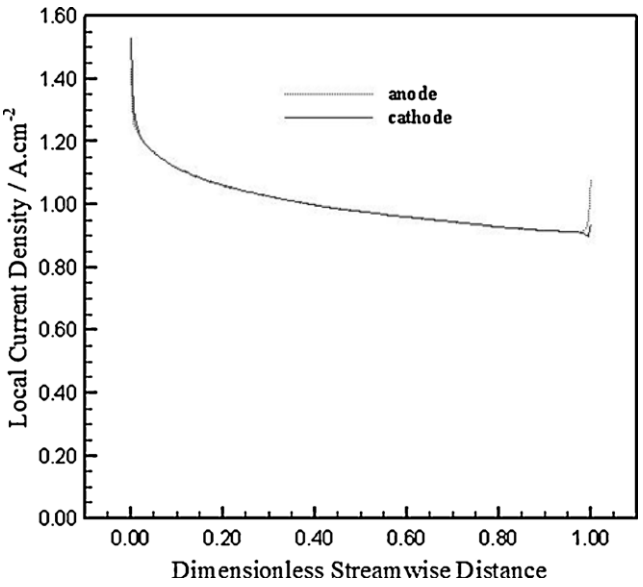

Fig. 3. Local current density along the electrodes at specified current density i = 1.0 A cm^{-2}, adiabatic boundary condition.

for all current densities examined except for low current densities, e.g., i < 0.2 A cm^{-2}. For a fixed current density, the KOH concentration decreases along the streamwise direction for i < 1.0 A cm^{-2}. However, for high current densities, e.g., i > 1.0 A cm^{-2}, the KOH concentration decreases sharply immediately downstream of the separator inlet and gradually increases toward the separator exit, consistent with the trend of the calculated local current density shown in Fig. 3. For the cathode, where OH^- is produced, the KOH concentration at fixed streamwise location increases with increasing current density. Along the cathode, the predicted KOH concentration was above the specified electrolyte concentration 7 M at the separator inlet. The results showed that it first increased and then decreased gradually along the cathode. The increase is due to the combined effects of high local current density at separator inlet, e.g., see Fig. 3, and loss of water to dry O_2 stream in the cathode gas channel. For i = 0.0 A cm^{-2}, loss of H_2O to dry gas channel due to evaporation results in KOH concentrations higher than 7 M. The results suggest that for low current densities the gas phase transport due to the loss of H_2O to gas streams is the predominant mechanism that determines the KOH concentration along the anode and cathode, whereas for high current density conditions, the reactant dissolving rates, the transport mechanisms and the electrochemical reaction rates are the predominant mechanisms.

4.2. Electric potential

The electric potential drop across the separator (liquid electrolyte) at specified current densities is shown in Fig. 4. The results show that the electric potential drop increases with increasing current density, and it reaches 0.07 V at the limiting current density 2.3 A cm^{-2}. In fact at 2.3 A cm^{-2} the electric potential drop across the electrolyte is comparable to that of the overpotential loss at the anode. More discussion on overpotential losses will follow. The simulation also shows that for high current densities (e.g., i > 1 A cm^{-2}) the electric potential drop jumps to a higher value immediate downstream of the separator inlet. The potential drop then decreases slightly at downstream locations. For low current densities, the electric potential drop decreases slightly along the streamwise direction.

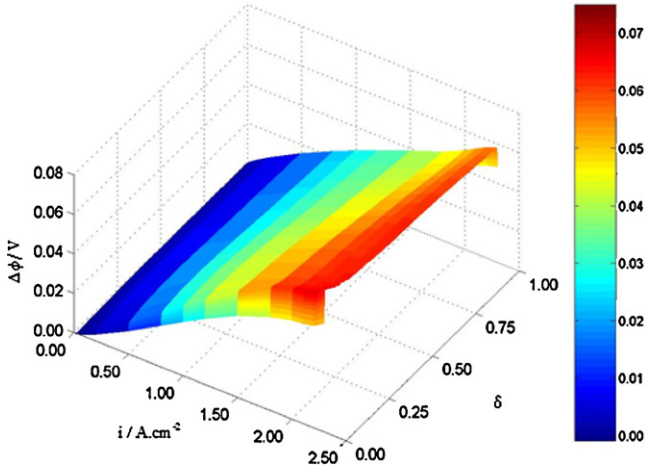

Fig. 4. Liquid-phase electric potential drop in KOH solution as functions of current density (i) and streamwise location (δ), adiabatic boundary condition.

The distribution of electric field potential in the liquid electrolyte is shown by the contour plot given in Fig. 5; the current density is set to 1 A cm^{-2}. It is noted that the presence of the electric field potential gradient in the streamwise direction leads to the development of shunt currents. The local primary current density decreases along the anode and cathode, but it remains the same at the anode and cathode for fixed streamwise locations (cf. Fig. 3). The decrease of current density along the streamwise direction is consistent with the decrease of reactant concentration

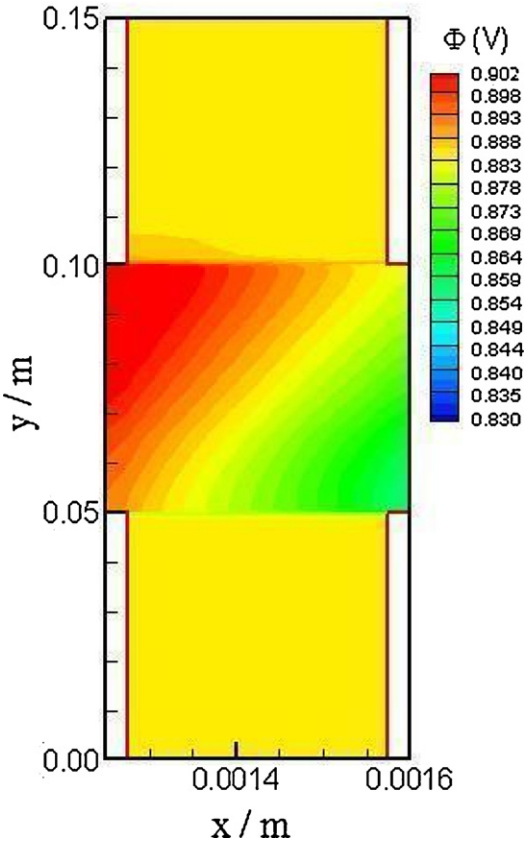

Fig. 5. Contour plot of liquid-phase electric potential in KOH solution at specified current density, i = 1 A cm^{-2}, adiabatic boundary condition. (For interpretation of the references to color in this figure legend, the reader is referred to the web version of the article.)

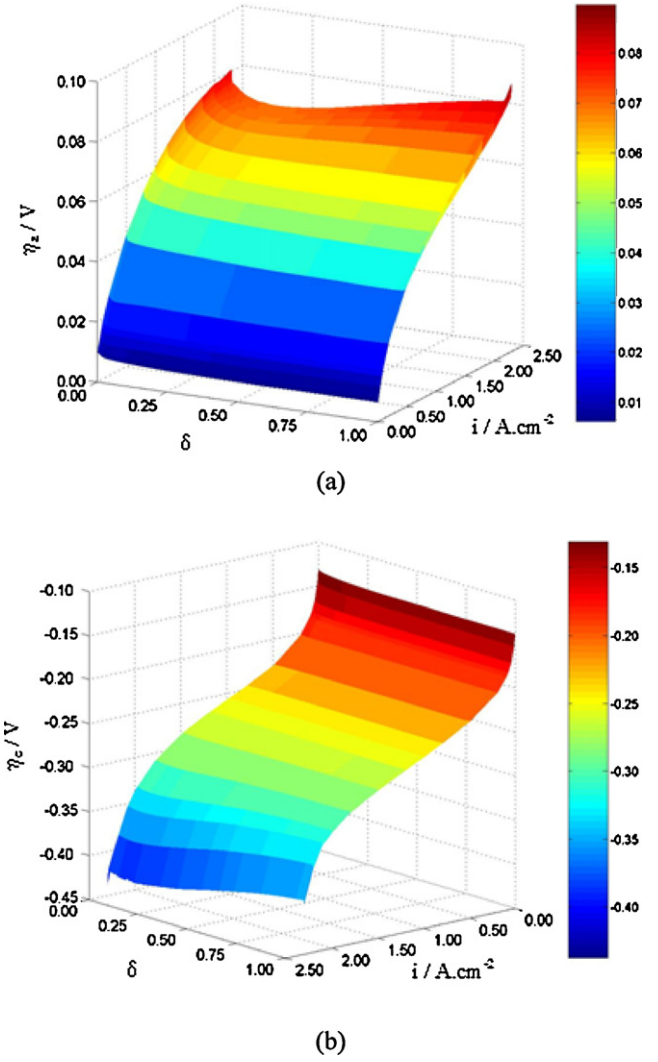

Fig. 6. Local overpotential at electrodes as functions of current density (i) and streamwise location (δ), adiabatic boundary condition; (a) anode and (b) cathode.

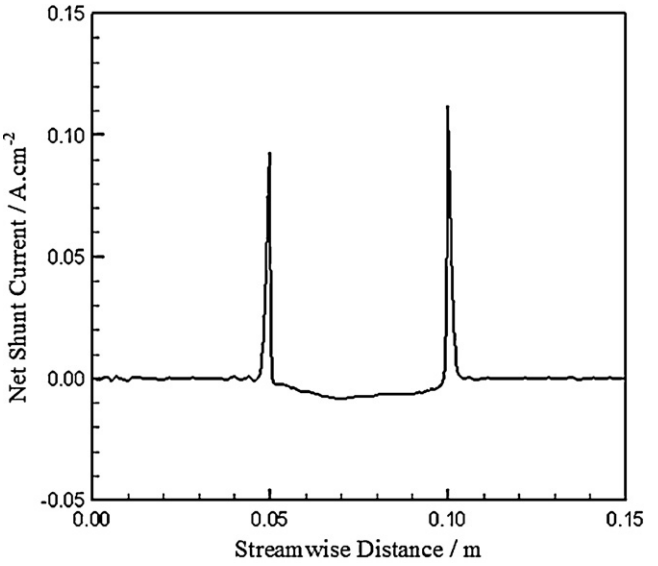

Fig. 7. Net shunt current density as a function of streamwise direction (δ) at specified current density i = 1 A cm^{-2}, adiabatic boundary condition.

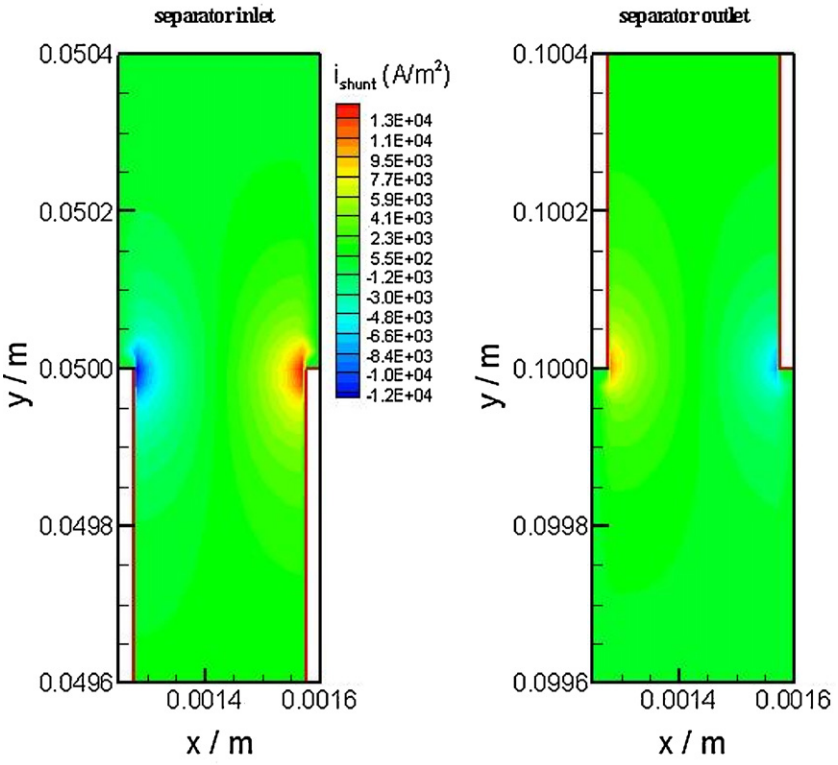

Fig. 8. Contour plot of shunt current density inside the separator ($0.05 \le y/m \le 0.10$) and extended channel at specified current density $i = 1\ A\,cm^{-2}$, adiabatic boundary condition; green color indicating zero shunt current. (For interpretation of the references to color in this figure legend, the reader is referred to the web version of the article.)

(i.e., H_2 and O_2) along the gas channels, suggesting that the species (i.e., OH^-) transport across the electrolyte is the predominant mechanism responsible for setting the local primary currents.

Distributions of the local overpotential at anode and cathode are shown in Fig. 6(a) and (b). The anode overpotential increases with increasing current density. But the overpotential remains relatively uniform in the streamwise direction. At low current densities (e.g., $i < 1\ A\,cm^{-2}$), the overpotential is highest at the separator inlet (i.e., $\delta = 0$), which is a result of the high local current density predicted (Fig. 3). At high current densities (e.g., $i = 2.3\ A\,cm^{-2}$),

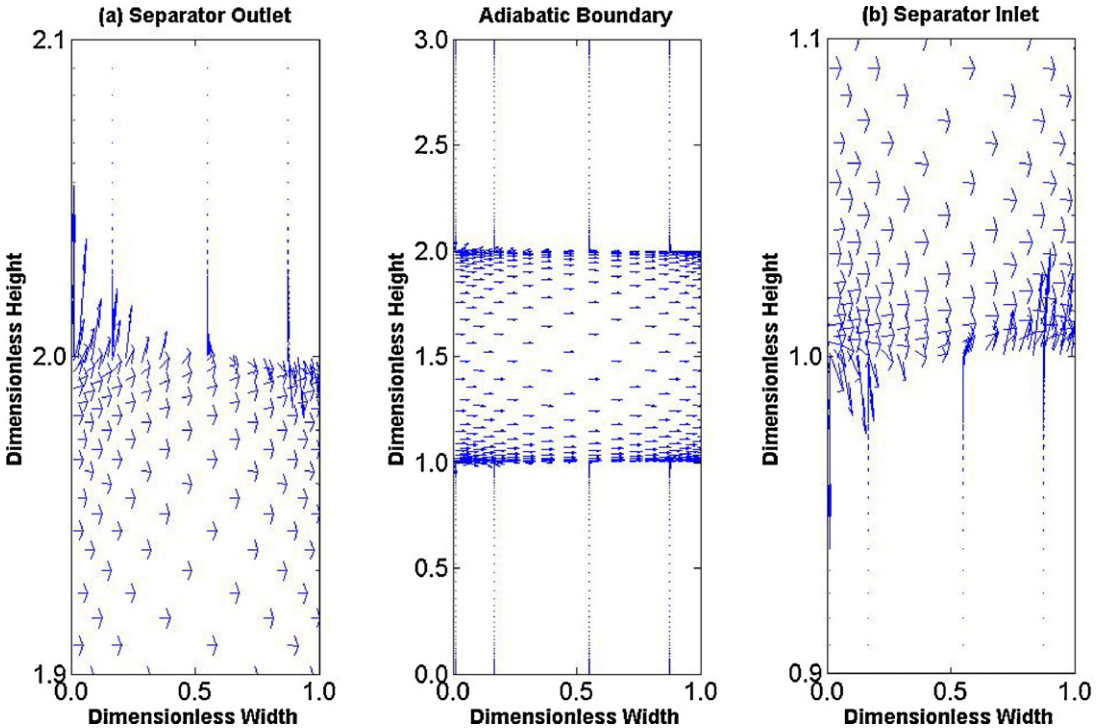

Fig. 9. Vector plot of current density inside separator and extended channel at specified current density $i = 1\ A\,cm^{-2}$, adiabatic boundary condition; vector length representing magnitude of the shunt current density.

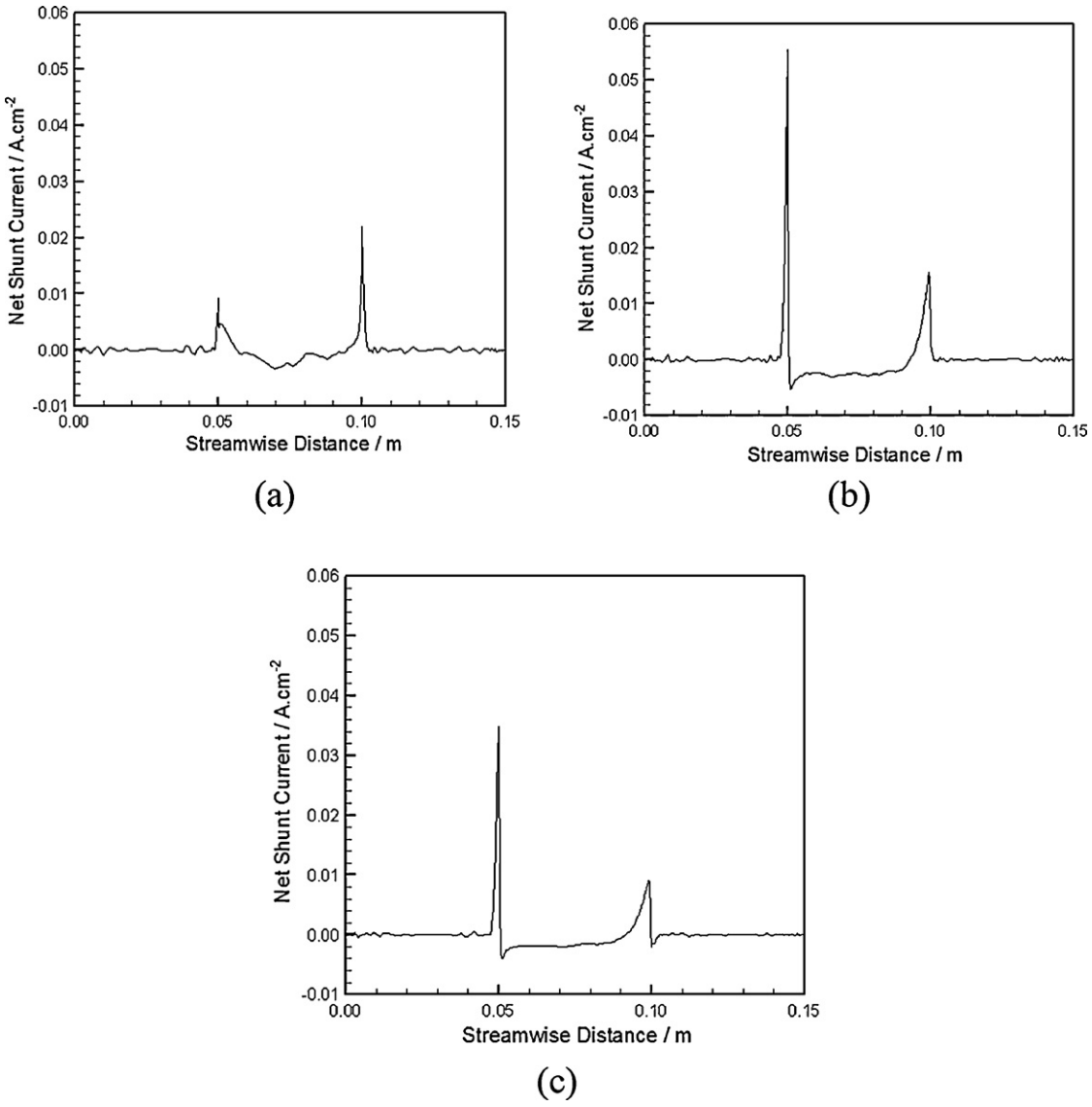

Fig. 10. Net shunt current density versus streamwise distance inside the separator (0.05 and 0.10 m) and in extended channel at specified current density $i = 1\,A\,cm^{-2}$; isothermal boundary condition: (a) 80 °C, (b) 50 °C, and (c) 25 °C.

the overpotential first decreases then increases along the streamwise direction, see Fig. 6(a). Similar trends were predicted for the cathode overpotential, except for high current densities (e.g., $i = 2.3\,A\,cm^{-2}$). At such conditions, the overpotential first increases then deceases toward the separator exit. It is noted that the cathode overpotential was significantly higher than the anode overpotential, 0.4 V versus 0.08 V, which is consistent with the well known fact that the cathode overpotential is the predominant loss mechanism. The low cathode exchange current density is responsible for the high overpotential at low current densities. At high current densities, availability of the reactants at cathode sets the overpotential losses, i.e., it is dominated by the cathode concentration overpotential.

4.3. Shunt current

4.3.1. Local and net shunt current

The net shunt current across the separator that accounts for the net ion fluxes in the streamwise direction is shown in Fig. 7. As shown, very low net shunt currents are predicted inside the separator and in the extended channels. Two peaks are predicted at the separator inlet and exit, i.e., at streamwise distances of 0.05 and 0.10 m, respectively. The calculated net shunt current densities are 0.09 and $0.11\,A\,cm^{-2}$ at the inlet and exit. The color coded local shunt current contours are plotted in Fig. 8. The results showed that the local shunt current density in the corner regions of the separator inlet and exit was as high as $1.8\,A\,cm^{-2}$. These large shunt current densities are to satisfy the electric potential equation in the regions adjacent to the separator inlet and exit. The vector plot of the current density is shown in Fig. 9. The expanded views at the separator exit and inlet are shown by inserts (a) and (b) in Fig. 9. At the separator inlet and exit, shunt currents are seen leaving the anode and returning to cathode. No current is observed in the extended channel. In the regions where shunt currents are present, electrolysis cells may form based on the local electric potential, pH value and material properties that lead to corrosion problems [34]. The results suggest that mitigation measures are needed to address potential corrosion problems near the separator inlet and exit.

To examine the effects of thermal boundary conditions on the presence of shunt currents, three isothermal boundary conditions were examined: (a) 80 °C, (b) 50 °C, and (c) 25 °C. As shown in Fig. 10, the peak shunt current density varies with varying thermal boundary conditions. The local shunt current density distribution, however, remains qualitatively similar for the adiabatic and

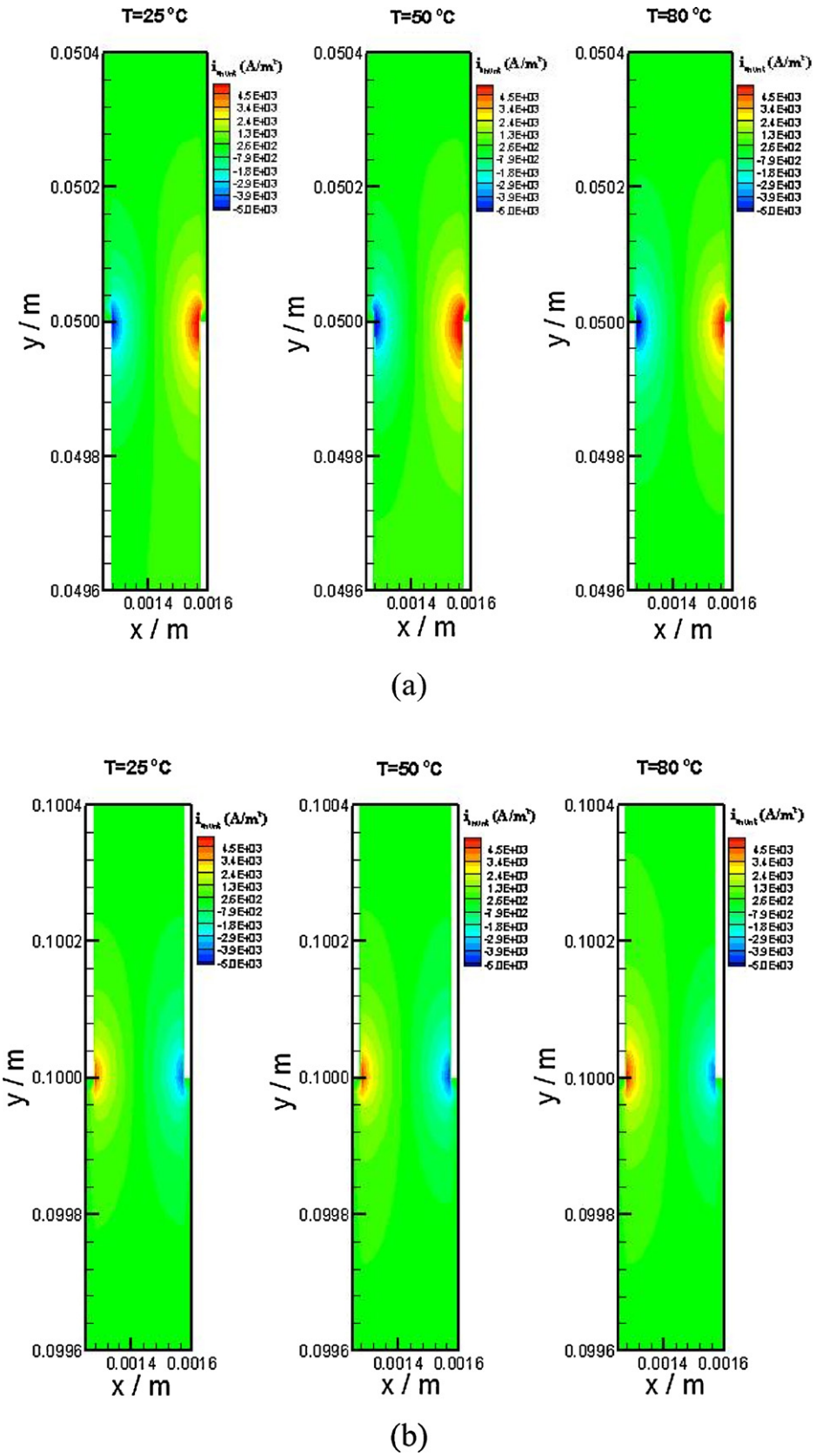

Fig. 11. Contour plot of shunt current density of isothermal boundary conditions (25, 50, or 80 °C) at specified current density $i = 1\ \mathrm{A\ cm^{-2}}$; (a) separator inlet and (b) separator outlet. (For interpretation of the references to color in this figure legend, the reader is referred to the web version of the article.)

isothermal boundary conditions considered, cf. Figs. 8 and 11. This finding suggests that shunt currents will be present regardless of the thermal boundary condition, and that thermal management will not be an effective means to mitigate the formation of shunt currents although it has a significant effect on the electrolyte transport [8].

4.3.2. Shunt current mitigation

The presence of large electric potential gradients in the separator inlet and exit regions is responsible for the presence of shunt currents, and potentially for forming electrolysis cells around the electrodes. The electrochemical redox reaction in the electrolysis cells is a source of corrosion [28,34]. To reduce the corrosion, passive and active preventive methods are developed. The passive method includes the application of protective coatings to the electrode surface in contact with the electrolyte, or placement of a porous barrier in electrolyte passages to increase the resistance in the regions of concern or to capture the net ionic fluxes leaving the separator. A review of the coating materials can be found in literature [35], and porous barriers or shields to prevent shunt current corrosion are reported in US patents [36–39]. The simulation results suggest that passive measures be applied in the separator inlet and exit regions. For the active protective methods, the simulation suggests an opposing voltage that counters the electric potential gradient in the electrolytes such as those reported in [28,40,41] should be applied immediately upstream of the separator inlet and downstream of the separator exit.

5. Summary and conclusion

A CFD study was conducted for the electrolyte transport in a single-cell alkaline fuel cell. The transport model accounts for the balance of mass, momentum, energy, species and electric charge in the electrolyte, and was solved using a commercial CFD software FLUENT®. The user defined functions were developed for calculation of the physical properties and the source terms of the governing equations, and to satisfy the prescribed boundary conditions.

The CFD study captured the presence of the primary and secondary (shunt) currents in the electrolyte of a single-cell alkaline fuel cell. The primary currents varied along the anode and the cathode and were highest at the separator inlet. The maximum local current density was more than 50% higher than the specified average current density. And identical local current densities were calculated for the anode and cathode everywhere but the separator exit where shunt currents were present. The following conclusions can be drawn:

1. The predicted local shunt current is in the regions where there exists a large electric potential gradient and where the primary current is lacking, i.e., in the regions adjacent to the separator inlet and exit. Shunt currents are not predicted in the extended channels.
2. Shunt currents are present regardless of applied thermal boundary conditions being adiabatic or isothermal (25, 50, and 80 °C).
3. The level of humidification of the reactant gas streams is important to KOH concentration at low current density conditions, through the loss of H_2O due to evaporation to gas channels.
4. At high current densities, the IR loss due to the electric potential drop is comparable to the overpotential loss at the anode; both are about an order of magnitude lower than the overpotential loss at the cathode.

Acknowledgments

This research was supported, in part, by ConocoPhillips through a research contract to The University of Iowa when Zhou and Chen were with the University of Iowa.

References

[1] K. Tomantschger, F. McClusky, L. Oporto, A. Reid, K. Kordesch, J. Power Sources 18 (1986) 317–335.
[2] K. Kordesch, V. Hacker, J. Gsellmann, M. Cifrain, G. Faleschini, P. Enzinger, R. Fankhauser, M. Ortner, M. Muhr, R.R. Aronson, J. Power Sources 86 (2000) 162–165.
[3] K. Strasser, J. Power Sources 29 (1990) 149–166.
[4] E.D. Geeter, M. Mangan, S. Spaepen, W. Stinissen, G. Vennekens, J. Power Sources 80 (1999) 207–212.
[5] T. Burchardt, P. Gouerec, E.S. Cortezon, Z. Karichevc, J.H. Miners, Fuel 81 (2002) 2151–2155.
[6] G.F. McLean, T. Niet, S. Prince-Richard, N. Djilali, Int. J. Hydrogen Energy 27 (2002) 507–526.
[7] L.M. Litz, K.V. Kordesch, Technology of hydrogen–oxygen carbon electrode fuel cells, in: G.J. Young, H.R. Linden (Eds.), Fuel Cell Systems, American Chemical Society, Washington, 1965, pp. 167–187.
[8] G. Zhou, L.-D. Chen, J.P. Seaba, J. Power Sources 196 (2011) 4923–4933.
[9] J.S. Newman, Electrochemical Systems, Eaglewood Cliffs, New Jersey, 1973.
[10] R.F. Probstein, Physicochemical Hydrodynamics: An Introduction, Butterworths, Boston, 1989.
[11] M.A. Al-Saleh, S. Gultekin, S. Rahman, A. Al-Zakri, J. Power Sources 55 (1995) 33–39.
[12] S.C. Yang, P. Bjornbom, Electrochim. Acta 37 (1992) 1831–1843.
[13] S. Rowshanzamir, M. Kazemeini, M.K. Isfahani, Int. J. Hydrogen Energy 23 (1998) 499–506.
[14] M.C. Kimble, R.E. White, J. Electrochem. Soc. 138 (1991) 3370–3382.
[15] J.H. Jo, S.C. Yi, J. Power Sources 84 (1999) 87–106.
[16] M. Katz, J. Electrochem. Soc. 125 (1978) 516–520.
[17] R.E. White, C.W. Walton, H.S. Burney, R.N. Beaver, J. Electrochem. Soc. 133 (1986) 485–492.
[18] H.S. Burney, R.E. White, J. Electrochem. Soc. 135 (1988) 1609–1612.
[19] H.N. Seiger, J. Electrochem. Soc. 133 (1986) 2002–2007.
[20] G. Bonvin, Ch. Comninellis, J. Appl. Electrochem. 24 (1994) 469–474.
[21] S.K. Rangarajan, V. Yegnanarayanan, Electrochim. Acta 42 (1997) 153–165.
[22] S.K. Rangarajan, V. Yegnanarayanan, M. Muthukumar, Electrochim. Acta 44 (1998) 491–502.
[23] E.R. Henquin, J.M. Bisang, J. Appl. Electrochem. 35 (2005) 1183–1190.
[24] E.A. Kaminski, R.F. Savinell, J. Electrochem. Soc. 130 (1983) 1103–1107.
[25] M.Z. Yang, H. Wu, J.R. Selman, J. Appl. Electrochem. 19 (1989) 247–254.
[26] A.T. Kuhn, J.S. Booth, J. Appl. Electrochem. 10 (1980) 233–237.
[27] G.W. Zhao, S.Z. Duan, Q.Z. Tian, T. Wu, Metall. Mater. Trans. B 21 (1990) 783–790.
[28] J.A. Schaeffer, L.-D. Chen, J.P. Seaba, J. Power Sources 182 (2008) 599–602.
[29] W.R. Parrish, J. Newman, J. Electrochem. Soc. 117 (1970) 43–48.
[30] J.B. Riggs, J. Electrochem. Soc. 80 (1980) 333 (Extended abstracts).
[31] V. Edwards, J. Newman, J. Electrochem. Soc. 134 (1987) 1181–1186.
[32] I. Rousar, J. Thonstad, J. Appl. Electrochem. 24 (1994) 1124–1132.
[33] W.B. Gu, C.Y. Wang, J.W. Weidner, R.G. Jungst, G. Nagasubramanian, J. Electrochem. Soc. 147 (2000) 427–434.
[34] T.P. Hoar, Atlas of Electrochemical Equilibrium in Aqueous Solution, second ed., National Association of Corrosion Engineers, Houston, 1974.
[35] N. De las Heras, E.P.L. Roberts, R. Langton, D.R. Hodgson, Energy Environ. Sci. 2 (2009) 206–214.
[36] R.P. Roche, P. Nowak, Integrated fuel cell stack shunt current prevention arrangement, U.S. Patent no. 5,079,104, 1992.
[37] R.P. Roche, Extruded fuel cell stack shunt current prevention arrangement, U.S. Patent no. 5,178,968, 1993.
[38] M. Katz, C.R. Schroll, Short protection device for stack of electrolyte cells, U.S. Patent no. 4,548,874, 1985.
[39] M. Zahn, P.G. Grimes, R.J. Bellows, Shunt current elimination and device, U.S. Patent no. 4,197,169, 1980.
[40] P.G. Grimes, M. Zahn, Shunt current elimination and device employing tunneled protective current, U.S. Patent no. 4,277,317, 1981.
[41] G. Zhou, Modeling and simulation of electrolyte transport in alkaline fuel cells, Ph.D. Thesis, The University of Iowa, Iowa City, 2007.